An Experimental and Theoretical Study of Multi-quantum Vibrational Excitation: NO(v = 0 → 1, 2, 3) in Collisions with Au(111)

Kai Golibrzuch[1], Alexander Kandratsenka[1,2], Igor Rahinov[3], Russell Cooper[1], Daniel J. Auerbach[1,2,4], Alec M. Wodtke[1,2,4], Christof Bartels[1*]

[1]Institute for Physical Chemistry, Georg-August University of Göttingen, Göttingen, Germany
[2]Max Planck Institute for Biophysical Chemistry, Göttingen, Germany
[3]Department of Natural Sciences, The Open University of Israel, Raanana, Israel
[4]Department of Chemistry and Biochemistry, University of California Santa Barbara
*Corresponding author: Christof Bartels, Tammannstrasse 6, D-37077 Goettingen, +49-551-3912599, cbartel@gwdg.de

Abstract

We measured absolute probabilities for vibrational excitation of NO ($v = 0$) molecules in collisions with a Au(111) surface at an incidence energy of translation 0.4 eV and surface temperatures between 300 K and 1100 K. In addition to previously reported excitation to $v = 1$ and $v = 2$, we observed excitation to $v = 3$. The excitation probabilities exhibit an Arrhenius dependence on surface temperature, indicating that the dominant excitation mechanism is nonadiabatic coupling to electron-hole pairs. The experimental data are analyzed in terms of a recently introduced kinetic model, which was extended to include four vibrational states. We describe a sub-population decomposition of the kinetic model, which allows us examine vibrational population transfer pathways. The analysis indicates that sequential pathways ($v = 0 \rightarrow 1 \rightarrow 2$ and $v = 0 \rightarrow 1 \rightarrow 2 \rightarrow 3$) alone cannot adequately describe production of $v = 2$ or 3. In addition, we performed first-principles molecular dynamics calculations that incorporate electronically nonadiabatic dynamics via an independent electron surface hopping (IESH) algorithm, which requires as input an *ab initio* potential energy hypersurface (PES) and nonadiabatic coupling matrix elements; both obtained from density functional theory (DFT). While the IESH-based simulations reproduce the $v = 1$ data well, they slightly underestimate the excitation probabilities to $v = 2$ and they significantly underestimate those for $v = 3$. Furthermore, this implementation of IESH appears to overestimate the importance of sequential energy transfer pathways. We make several suggestions concerning ways to improve this IESH based model.

Keywords: nonadiabatic, surface scattering, IESH, multi-quantum vibrational excitation

1. Introduction

Molecular-level studies of the fundamental energy transfer processes at gas-solid interfaces are crucial for a predictive understanding of such important processes as heterogeneous catalysis, etching and corrosion. The inter-conversion of energy between molecular vibrations and lattice degrees of freedom is particularly important as vibration can be directly related to the dissociative reaction coordinate. There is a growing body of experimental and theoretical evidence that when molecules interact with metallic surfaces, the adiabatic (Born-Oppenheimer) approximation breaks down and molecular vibration can couple to electron-hole pair (EHP) excitations of the metal [1]. Particularly extensive data is available for electronically nonadiabatic coupling of nitric oxide (NO) with various metal surfaces, including work on both vibrational relaxation [2] and excitation [3].

Several theoretical approaches were successful in at least qualitatively describing electronically nonadiabatic vibrational relaxation [4]. Obtaining *quantitative* agreement is more challenging using a first-principles approach [5]. Recently, semi-quantitative agreement was obtained between experimental data and an independent-electron surface hopping (IESH) based model, over a wide range of surface temperatures, T_S, and incidence energies for vibrational excitation observed in the NO(v=0→1,2)/Au(111) system.[6]

Despite this success, deviations remain between the theoretical predictions of the IESH-based model and experimental observations. In particular, the simulations underestimate the incidence energy dependence of the vibrational excitation probabilities. While the measured excitation probabilities increase with incidence energy, the calculated values are almost constant. In addition, the theory slightly underestimates the T_S dependence of the vibrational excitation probabilities.

In this study, we extend our investigation of vibrational excitation of NO on Au(111). Recent experimental improvements allow us to observe transitions from $v = 0$ to $v = 3$ upon collision with the gold surface with high signal-to-noise ratio. This provides a stronger benchmark against which theories of electronically nonadiabatic interaction can be tested. We use this data to further test predictions of the highly successful IESH-based model. We find that the IESH-predicted excitation probabilities are increasingly in error as Δv increases. We examine some of the possible reasons behind this.

Another important question addressed in this paper concerns whether vibrational energy transfer of NO with Au occurs via single or multiple electronically nonadiabatic energy exchange events. That is, does the multi-quantum vibrational excitation of NO (v = 0→3) occurring on a sub-picosecond time scale during a direct scattering process occur in a single step (overtone) or as a result of several (sequential) steps. Vibrational promotion of electron emission seems to require that high overtone processes play an important role at least under some conditions, e.g. relaxation of highly vibrationally excited NO on Cs overlayers on Au(111)[2b]. Many assume that the better theoretically understood NO/Au system behaves similarly; but, this remains to be demonstrated. To help clarify this issue, we also compared the IESH model to a previously reported state-to-state kinetic model[7] that is a simple means of mechanistic data analysis, whereby we obtain information on sequential, direct-overtone and hybrid channels. This sheds further light on some of the weaknesses of the IESH-based simulations, which appears to underestimate the importance of overtone transitions. We make several suggestions how this theoretical approach might be improved.

2. Methods

2.1 Experimental setup

A detailed description of the experimental setup has been published previously [8]. Briefly, a pulsed molecular beam is generated using supersonic expansion of a gas mixture (15.5% NO in H_2) at 3 atm. stagnation pressure into vacuum through a piezoelectrically operated valve. The mean translational energy of the beam is determined to be 0.4 eV using a double resonance IR-UV scheme, where the incident beam of NO molecules is vibrationally tagged using a 1.8 μm infrared laser, and the excited molecules are detected 18 mm downstream [9].

The molecular beam passes through two stages of differential pumping before it enters an ultra-high vacuum chamber, where it is scattered from a single-crystal Au(111) surface. The surface is cleaned using Argon ion sputtering, and its cleanliness is verified with Auger electron spectroscopy. The surface is subsequently annealed at about 1000 K for 30 minutes to recover the (111) surface structure.

The scattered molecules are state-specifically ionized using resonance enhanced multiphoton ionization (REMPI), and the ions are collected using an ion collection system consisting of a repeller and an electrostatic focusing lens with two cylindrical

elements, and detected on a two-stage microchannel plate (MCP). One-color (1+1) REMPI of NO was accomplished via $A^2\Sigma(v'=0) \leftarrow X^2\Pi(v''=0,1,2)$ transitions using the frequency-doubled output (laser pulse energy 0.2–3 mJ) of a tunable dye laser pumped by the third harmonic of a Nd:YAG laser.

The $A(v'=0) \leftarrow X(v''=0, 1, 2, 3)$ bands were chosen due to their spectral isolation, allowing us to integrate the measured REMPI intensity over the entire rotational distribution of a specific vibrational state. For measurements of NO($v=1$), the influence of a small background from thermally populated NO($v=1$) present in the incident beam was determined by extrapolating the T_S surface temperature dependence of the NO($v=1$) signal to $T_S = 0$ K. This allowed this source of background to be systematically subtracted from all data [10].

For the scattered NO($v=3$) observed in this work, the detection efficiency of the one-color (1+1) REMPI scheme is not high enough for high-quality absolute excitation probability measurements. This is due to the low probability of $v=3$ excitation and low signal for detection of $v=3$ by (1+1) REMPI. Attempts to increase the signal by simply increasing the photon flux failed because this leads to significant background signal form non-resonant two-photon ionization. The detection efficiency can be improved using a two-color (1+1') REMPI scheme[11], where two separate lasers are used for resonant excitation (tunable wavelength, 1–3 mJ/pulse) and for ionization (fixed wavelength, 14 mJ/pulse). The ionization step is realized with the fourth harmonic (266 nm) of a Nd:YAG laser. This detection scheme results in a signal enhancement factor of 3–5 in comparison to traditional (1+1) REMPI of NO via the A-state.

The temperature of the gold crystal is adjusted by resistive heating of tungsten wires to which it is mounted. Its temperature is measured using a type K thermocouple attached to the crystal. Experiments are performed for surface temperatures between 300 K and 1100 K.

For each value of T_S, we record rotationally resolved spectra via the $A(v'=0) \leftarrow X(v''=0, 1, 2, 3)$ bands, and temporal and angular distributions of scattered NO molecules for each vibrational state. The temporal distributions are measured by varying the delay between the pulsed nozzle and the laser pulses, and the angular distributions are measured by translating the laser beam(s) parallel to the

surface. Absolute excitation probabilities are then calculated from these data according to the protocol outlined in a recent publication[10].

2.2 State-to-state kinetic model

In order to quantitatively assess the relative importance of direct-overtone versus sequential paths of multi-quantum excitation, we analyze the data using a previously introduced state-to-state kinetic model [7], which we extended from three to four vibrational states; that is, v = 0, 1, 2 and 3. Here, we allow for all possible permutations of single and multiple quantum excitation and relaxation processes to proceed concurrently, assembling a system of differential equations that combines all possible excitation and relaxation pathways:

$$\frac{dn_v}{dt} = \sum_{\substack{v'=0 \\ v' \neq v}}^{3} (k_{v'v} n_{v'} - k_{vv'} n_v) \qquad (1)$$

In this system of rate equations, n_v is the instantaneous population in the vibrational state v and $k_{vv'}$ is the rate constant for a transition from v to v'. The vibrational transition rate constants are determined from Fermi's Golden Rule, taking into account the finite temperature of the surface which governs the availability of thermally excited EHPs [7]:

$$k_{vv'} = \alpha_{vv'} \frac{\Delta E_{vv'}}{\exp\left(\frac{\Delta E_{vv'}}{k_B T_S}\right) - 1} \qquad (2)$$

where $\alpha_{vv'}$ can be related to the perturbation matrix element coupling the electronic and vibrational degrees of freedom; see Ref. 7.

Of course in this four level analysis, the experimental data are not sufficient to allow an unambiguous determination of all state-to-state rate constants. In order to reduce the number of fitting parameters in our model, we take the following steps. First of all, we utilize the detailed balance condition for the coupling coefficients ($\alpha_{vv'} = \alpha_{v'v}$). We then must assume a v-scaling law for $\alpha_{vv'}$. In order to evaluate the impact of this scaling law assumption, we carry out analysis for two very different assumptions concerning the scaling law; which we subsequently refer to as case (a) and case (b). In case (a) we assume that $\alpha_{vv'}$ is independent of v. For case (b) we

assume $\alpha_{vv'}$ is linearly proportional to v. For example, this means that $\alpha_{32} = 3\alpha_{10}$. Case (b) is commonly used when one assumes a linear coupling of a harmonic oscillator to a thermal bath of states. See, for example, Ref. 4b.

This can be expressed more precisely as follows. We introduce scaling parameters α_v, β_v and γ_v expressing the relative importance of state-to-state transitions:

$$\begin{aligned} \alpha_{v,v\pm1} &= \alpha_i \alpha_{0,1} \\ \alpha_{v,v\pm2} &= \beta_i \alpha_{0,1} \\ \alpha_{v,v\pm3} &= \gamma_i \alpha_{0,1} \end{aligned} \qquad (3)$$

Here, the index i refers to case (a) or (b). Case (a) corresponds to $\alpha_a = 1, \beta_a = \beta$, and $\gamma_a = \gamma$. Case (b) on the other hand, corresponds to, $\alpha_b = v + 1$, $\beta_b = (v + 1)\beta$, and $\gamma_b = (v + 1)\gamma$. Here β and γ are constants that are varied to fit experimental data, and describe the relative contributions of direct 1st and 2nd overtone processes.

As described in Ref. 7, we cannot independently determine the interaction time, t_{int}, and the coupling parameter, $\alpha_{0,1}$, based on the absolute excitation probability data alone. Therefore, we combine them into a new parameter $\tau = \alpha_{0,1} t_{int}$ with dimensions of inverse energy. The solution of the rate equations with the appropriate initial conditions then yields the vibrational populations $n_v(T_S; \tau, \beta, \gamma)$ for each experimental value of T_S. The parameters τ, β and γ are optimized to fit the complete data set or absolute excitation probabilities.

2.3 Sub-population Analysis

Solving the differential master equations (1) yields expressions for the evolution of the populations of the available vibrational levels with time, $n_v(t)$. However, it is not possible from these equations alone to know the pathway that was followed to reach a given final level. For example, excitation to $v = 3$ can occur by a direct-overtone process, $0 \rightarrow 3$, by two hybrid pathways, $0 \rightarrow 1 \rightarrow 3$ and $0 \rightarrow 2 \rightarrow 3$, and by a sequential pathway $0 \rightarrow 1 \rightarrow 2 \rightarrow 3$. For completeness we note that there is an infinite number of other more complex pathways, like $0 \rightarrow 1 \rightarrow 2 \rightarrow 1 \rightarrow 3$. We will show below that the sequential, hybrid, and direct-overtone pathways are significantly more probable than these complex pathways. Once we have used the kinetic model to fit experimental results – that is, we experimentally derive τ, β and γ under either case (a) or case (b) – it is possible to determine the relative importance of these pathways.

To accomplish this determination, we decompose the population in each level into a sum of populations that arise by some specific pathway:

$$n_v(t) = n_v^{(0)}(t) + \sum_{v_1 \neq v} n_{v_1 v}(t) + \sum_{\substack{v_1 \neq v \\ v_2 \neq v_1}} n_{v_1 v_2 v}(t) + \cdots \tag{4}$$

where $n_v^{(0)}(t)$ denotes the time-dependent sub-population of level v resulting from the *t=0* population in state v; $n_{v_1 v}(t)$ is the sub-population of the level v formed by the single-step transition from the level v_1; $n_{v_2 v_1 v}(t)$ is the sub-population of the level v gained due to the two-step transition $v_2 \to v_1 \to v$, and so on.

By writing kinetic master equations for these sub-populations and by solving them we obtain information on the pathways that lead to a given level. The initial sub-population $n_v^{(0)}(t)$ of a level v, which is not formed by transitions from other states, can only decrease due to the population transfer to other levels:

$$\frac{dn_v^{(0)}}{dt} = -\kappa_v n_v^{(0)}, \qquad \kappa_v = \sum_{v_1 \neq v} k_{v v_1} \tag{5}$$

where the total outgoing rate is denoted by κ_v.

The master equation for the single-step sub-population $n_{v_1 v}$ of the v^{th} level entering Eq. (4) is constructed by counting the gain due to the initial sub-population of the level v_1 and the loss into other levels.

$$\frac{dn_{v_1 v}}{dt} = -\kappa_v n_{v_1 v} + k_{v_1 v} n_{v_1}^{(0)} \tag{6}$$

The same structure is preserved for differential equations governing the time evolution of any α-step sub-population $n_{v_1 \ldots v_\alpha v}$ of the level v:

$$\frac{dn_{v_1 \ldots v_\alpha v}}{dt} = -\kappa_v n_{v_1 \ldots v_\alpha v} + k_{v_\alpha v} n_{v_1 \ldots v_\alpha} \tag{7}$$

where $k_{v_\alpha v}$ is the $v_\alpha \to v$ transition rate constant and $n_{v_1 \ldots v_\alpha}$ is the $(\alpha - 1)$-step sub-population of the level v_α.

Eqs. (5)-(7) form a chain of differential equations which completely define the time evolution of all sub-population contributions into the total population (4). Differentiating (4) with respect to time, it is easy to show that these equations are identical to the master equation (1).

The constructed system of the sub-population differential equations can be solved analytically. We start from the eq. (5) yielding the exponential decay for the initial sub-population:

$$n_v^{(0)}(t) = n_v^{(0)}(0)\mathrm{e}^{-\kappa_v t} \tag{8}$$

where $n_v(0)$ is the initial population of the level v. Then eq. (6) can be considered as a non-homogeneous linear equation for the single-step sub-population with initial condition $n_{v_1 v}(0) = 0$ which has the following solution.

$$n_{v_1 v}(t) = n_v^{(0)}(t)\mathrm{e}^{-\kappa_v t}\frac{\mathrm{e}^{-(\kappa_v - \kappa_{v_1})t} - 1}{\kappa_v - \kappa_{v_1}} \tag{9}$$

Equation (9) can be used as input to solve the differential equation defining the time evolution of the 2-step sub-population for level v, and so on for sub-population of any order.

To reiterate, the presented sub-population formalism serves as a general framework for quantitative analysis of the energy transfer pathways from the scattered molecule into the surface. By obtaining a set of state-to-state rate constants – those of Eq. (1) – by fitting experimental data and assuming either case (a) or case (b), we may reconstruct the subpopulation excitation pathways. By comparing results obtained under case (a) and case (b) we can evaluate the errors associated with this analysis.

2.4 Independent-Electron Surface Hopping Theory

For first-principles modeling of NO/Au(111) electronically nonadiabatic dynamics, we use the IESH approach described in detail in Ref. [12], which is a direct extension of the original surface hopping algorithm [13] to a molecule-surface collision case. Briefly, in this approach a molecule-surface system is described in terms of the many-electron Newns-Anderson Hamiltonian [5a]. Here the electronic state of the NO molecule is represented by an affinity orbital and the metal continuum is modeled by a set of M_S

discrete states obtained as solutions of the corresponding Schrödinger equation using Gaussian quadrature [14]. Multi-dimensional potential energy surfaces describing the interaction of neutral and ionic molecular states with the surface as well as the coupling function between adsorbate and metal orbitals were determined by means of DFT calculations, which were fitted by a set of physically reasonable pair potentials. In particular, a Morse potential function was used for the NO vibration [12b]. It is important to note that the PES and nonadiabatic couplings used in this work are the same as those used in previous IESH studies of NO on Au(111)[6,12].

The main advantage of the IESH method is the calculationally effective explicit description of the nonadiabatic dynamics of electrons of the metal conduction band including multiple EHP excitations without restriction to a small subset of the excited electronic states. This feature allows us to obtain hundreds of thousands of trajectories with nonadiabatic dynamics with a moderate computational cluster in a reasonable time, which makes it possible for the IESH theory to directly simulate rare events like NO vibrational excitations due to the collisions with a metal surface. So, the comparison of the measured values for NO vibrational 0→1 and 0→2 excitation probabilities for a wide range of incidence energies and surface temperatures with calculated values proved the capability of the IESH approach to capture the underlying physics at the scattering process under consideration [6]. In particular, IESH simulations support the view of the importance of electron transfer mediated nonadiabatic effects for NO vibrational energy exchange with Au(111), effects that go beyond the level of the "electronic friction" theory. Relying on the above-mentioned effectiveness of the IESH algorithm, we can now extend our study by calculating the NO vibrational 0→3 excitation probability and comparing the results to the measured values. Since this probability of 0→3 excitation is quite low (of order 10^{-5}), it was necessary to calculate at least one million trajectories (10 times more trajectories than in our previous report[6]) for each value of surface temperature.

One of the important parameters in the IESH model is the number of discrete energy levels, M_S, representing the metal continuum[12a]. Of course, the more levels, the better; however, the computational cost scales very unfavorably with this number. Our current cluster makes it possible to produce 10^5 trajectories with incidence energy of 0.4 eV and surface temperature 800 K in about three days for $M_S = 80$, whereas it takes more than two weeks for $M_S = 160$. We address the influence of the number of

metal electronic states on the calculated vibrational excitation probabilities in Section 3.5.

As the NO vibration was propagated classically, an issue of quantum-classical correspondence arises when calculating the vibrational transition probabilities. We used the Bohr-Sommerfeld quantization rule [15],

$$h\left(v_{\mathrm{cl}}+\tfrac{1}{2}\right)=\oint p_r dr \qquad (10)$$

where p_r is the momentum conjugate with the vibrational coordinate r and the integral is taken over a period of vibration. Surprisingly, for the rotating Morse oscillator, which models the NO vibration in our case, this integral can be calculated analytically yielding the classical action as a function of NO rotational and vibrational energy [16]. The vibrational action in the left-hand side of Eq. (10) is written in terms of the classical analog v_{cl} of the quantum number, which is determined for a given trajectory from the values of NO rotational and vibrational energy after collision with the Au(111) surface. In order to calculate the vibrational $0 \rightarrow v$ excitation probabilities we sum the contributions from trajectories with $v-\frac{1}{2} \leq v_{\mathrm{cl}} \leq v+\frac{1}{2}$ (box binning).

3. Results and Discussion

3.1 Angular distributions

Angular distributions for scattered NO(v) molecules are shown in Fig. 1. The distributions are nearly identical for scattered molecules in all four vibrational states. They all peak at the specular angle (3.3° from the surface normal) and are well described by a narrow $\cos^{10.1}(\theta+3.3°)$ distribution. This is clear experimental evidence indicating that vibrational excitation happens in a direct single-bounce scattering process for $v=0 \rightarrow 1, 2$ and 3. A trapping-desorption mechanism, which would appear as a $\cos^2\theta$ distribution under our experimental conditions [17], can be excluded.

3.2 Absolute vibrational excitation probabilities

Typical rotationally resolved REMPI spectra of the scattered NO($v=0$) → NO($v'=0-3$) molecules for T_S =973K are presented in Fig. 2. These spectra are corrected for differences in MCP gain, laser power and two-color REMPI enhancement. By

inspection of Fig. 2 one can immediately estimate the magnitudes of the absolute excitation probabilities to be ~ 1×10^{-2}, 4×10^{-4} and 2×10^{-5} for NO($v = 0$) → NO($v' = 1, 2, 3$) scattering events, respectively. Take note that the NO($v = 0$) spectral intensity is nearly independent of T_S. [17]

Spectra like those shown in Fig. 2 were recorded at surface temperatures ranging from 300 to 1100 K. In order to rigorously derive the absolute vibrational excitation probabilities, the integrated spectral intensities were converted from density-to-flux by the proper Jacobian and corrected for differences in temporal and angular distributions, laser power and detector gain to obtain the corrected spectral intensities of the corresponding spectral bands, S_v. Ratios of these corrected signal intensities, $S_{1,2}$, to the corrected spectral intensity of the vibrational ground state, S_0, yield the absolute excitation probabilities P_{01} and P_{02}. Details for this procedure are given in Ref. [17].

The probabilities for $v = 0 \rightarrow 3$ excitation, P_{03}, were found in a similar way but with an additional correction factor taking into account the increased sensitivity of the two-color REMPI scheme used to detect the scattered NO(v=3) molecules. For this correction, additional data sets were recorded for scattered NO($v = 2$) using two-color REMPI, which were then compared to the one-color REMPI data to give the signal enhancement for NO($v = 2$). The NO(v=2) state was used for this purpose because both one and two-color REMPI schemes provide good S/N ratio for that state leading to more precise quantitative results. From the integrated spectral intensities, we obtained the two-color/one-color scaling factor assuming the ionization cross section to be independent on the ionization wavelength[18]. Data for NO($v = 0$) → NO($v' = 3$) were then recorded using two-color (1+1') REMPI.

The resulting probabilities for excitation to $v = 1, 2, 3$ are shown in Figure 3. Consistent with the rough estimates described above, we find that the absolute excitation probabilities are in the ranges of P_{01}~$10^{-3}\ldots10^{-2}$, P_{02}~$10^{-4}\ldots10^{-3}$, P_{03}~$10^{-5}\ldots10^{-4}$ with a strong T_S − dependence. For any given temperature, P_{02} is more than one order of magnitude smaller than P_{01}, and P_{03} is at least another order of magnitude smaller than P_{02}.

3.3 Arrhenius pre-exponential factors

It has been previously shown that for NO($v = 0$) scattering from Au(111), the probabilities for $v = 1,2$ excitation follow an Arrhenius-like surface temperature dependence with activation energies equal to the respective vibrational excitation energies:[3a, 3c]

$$P_{0v} = A_{0v} \exp\left(-\frac{\Delta E_{0v}}{k_B T_S}\right) \qquad (11)$$

The T_S dependent data for $v = 1, 2$ and 3 obtained in this work also follow the form of Eq. (11); see Figure 3, solid lines. Such temperature dependence is indicative of the vibrational excitation resulting from thermally excited EHP relaxation.[3]

In Eq. (11), the pre-exponential factor A_{0v} is related to the intrinsic coupling strength between EHPs and molecular vibration, while the exponential term represents the statistical likelihood to find a thermally excited EHP with sufficient energy to excite molecular vibration [7]. From the least-squares fits with fixed slopes [3c], we obtain the following pre-exponential factors: $A_{01} = 0.35 \pm 0.01$, $A_{02} = 0.24 \pm 0.01$ and $A_{03} = 0.16 \pm 0.01$ for the three vibrational channels. The fact that these quantities are so similar indicates similar intrinsic coupling strengths for all three vibrational excitation channels. That is, the main reason for the reduced excitation probabilities with increasing final vibrational quantum number is the reduced population of appropriately energetic thermally populated EHPs.

This can be seen as well by considering the thermal limits also shown in Fig. 3 as dashed lines. The thermal limit for vibrational excitation for a harmonic oscillator (or for an anharmonic oscillator – see appendix) is given by Eq. (12).

$$P_{\text{therm}}(\Delta E_{0v}) = \exp\left(-\frac{\Delta E_{0v}}{k_B T_S}\right)\left[1 - \exp\left(-\frac{hc\omega_e}{k_B T_S}\right)\right] \qquad (12)$$

The thermal limit is the excitation probability that would result from a complete thermalization of the vibrational degree of freedom of the molecule with the surface; that is, the highest vibrational excitation probability observable if vibrational excitation occurs by conversion of thermal energy of the solid to NO vibration, i.e. if T-V excitation is unimportant. In a forthcoming publication we will show that the assumption of weak T-V coupling is a good one. In the low-temperature limit, [7] which is valid over the temperature range of this work, Eq. (12) is equivalent to an Arrhenius

curve with pre-factor of 1. The pre-exponential factors presented above vary between 0.35 and 0.16.

3.4 Kinetic Model: Population Transfer Pathways

This can be understood in more detail using the state-to-state kinetic model [3c, 7], described in Sec. 2.2 and supplemented by the sub-population analysis from Sec. 2.3. The system of linear differential rate equations (1) is solved numerically in the 4-level system using the standard procedure (NDSolve) with Mathematica 8.0 package.

As described above in Sec. 2.2, specifically the text surrounding Eq. (3), we carry out this fit for two assumptions concerning the v-scaling of the state-to-state nonadiabatic coupling. In both cases we fit the model globally to the experimental data by simultaneous minimization of the weighted squared deviations for three data sets for $v = 1, 2$ and 3 using τ, β and γ as fit parameters. This fit yields

$$\begin{aligned} \tau_a &= (1.797 \pm 0.004)\ \text{eV}^{-1},\ \beta_a = (0.289 \pm 0.002),\ \gamma_a = (0.103 \pm 0.006) \\ \tau_b &= (1.806 \pm 0.005)\ \text{eV}^{-1},\ \beta_b = (0.243 \pm 0.003),\ \gamma_b = (0.014 \pm 0.010) \end{aligned} \qquad (13)$$

The subscripts a and b refer to the two v-scaling laws for nonadiabatic coupling. See section 2.2. The errors indicate 99.9% confidence intervals ($\Delta\chi^2 = 6.63$) assuming the normal distribution of error in the data.

The resulting curves are shown in Fig. 4. As is clearly seen from the figure, the kinetic model fits the experimental data very well. Furthermore, case (a) and case (b) work equally well to fit the data despite their very different assumptions about v-scaling. Hence, it is immediately clear that the data presented in this paper are not capable of distinguishing between case (a) and case (b) and we interpret our findings only to the extent that case (a) and case (b) results are in agreement with one another. In future work, we hope to obtain new experimental results characterizing the v-scaling of the state-to-state nonadiabatic coupling.

By setting β and/or γ to zero, we may see the importance of first and second overtone transitions in excitation to v = 2 and 3. For example, the excitation from $v = 0 \rightarrow v = 3$ may have some contribution from direct-overtone transitions, which can be switched off in the kinetic model by setting $\gamma = 0$ and evaluating it again. When this is done, the kinetic model in case (a) deviates from experiment (dot-dashed line in Fig. 4). For case (b) scaling, agreement with experiment is maintained for $\gamma = 0$.

Hence, until we know more about the relative validity of case (a) versus case (b), we cannot conclude from this analysis alone that direct overtone $v = 0 \rightarrow 3$ transitions are important for populating v=3.

On the other hand, by setting both $\beta = 0$ and $\gamma = 0$ and refitting, we may estimate the importance of a purely sequential mechanism ($v = 0 \rightarrow 1 \rightarrow 2 \rightarrow 3$). Here, the kinetic model completely fails to reproduce either $v = 2$ or $v = 3$ measured excitation probabilities. This is true both for case (a) and case (b). See Fig. 4. Hence we conclude that it is crucial to include hybrid and/or direct overtone transitions in order to understand the experimental data. This conclusion is consistent with the previous analysis of experimental results on $v = 1,2$ excitation with a 3-state model, which indicated that $v = 2$ is populated via a direct-overtone ($0 \rightarrow 2$) rather than a sequential ($0 \rightarrow 1 \rightarrow 2$) pathway [3c,7].

Of course, these conclusions are semi-quantitative in nature, since reevaluation under constrained, e.g. $\beta = 0$ and/or $\gamma = 0$, conditions is artificial. We may obtain more precise understanding of our results be applying our method of sub-population analysis for both case (a) and case (b), which is derived from an unconstrained fit to the data. This allows us to address questions like: 1) to what extent is $v = 2$ populated by sequential versus a direct-overtone mechanism, 2) to what extent is $v = 3$ populated by sequential versus hybrid versus direct-overtone mechanisms. The magnitudes derived for NO v = 2 and 3 from our sub-population analysis are collected in Table 1.

Fig. 5 shows the calculated sub-populations of levels v =1-3 as functions of time represented by a dimensionless variable $\alpha t = \hbar\omega_0\alpha_{01}t$ with ω_0 denoting the NO harmonic frequency. The vertical dashed lines show the values of αt that fit the data optimally. Plots in the left column show results following from case (a) and plots in the right column correspond to those from case (b). The kinetic model description of v=1 excitation (upper panels in Fig. 5) is, of course, quite simple, both for case (a) and (b). There is only one relevant sub-population n_{01} which represents a single-step transition from $v = 0 \rightarrow 1$. This contributes 99% of the total population to $v = 1$. The unaccounted for 1% sub-population results from pathways like $v = 0 \rightarrow 2 \rightarrow 1$ and $v = 0 \rightarrow 3 \rightarrow 1$.

The middle panels of Fig. 5 show similar results for $v = 2$ production. Two sub-populations n_{02} (due to a direct-overtone pathway from the ground state) and n_{012} (due to a 2-step sequential pathway) are both important for producing the second excited level. Their relative contribution depends only weakly on the choice of case (a) or case (b). See Fig. 5 and Table 1.

The lower panel of Fig. 5 shows the same analysis for production of $v = 3$. Here four contributions are identified: n_{03} (reflecting the importance of the direct-overtone pathway $0 \rightarrow 3$); n_{013} and n_{023} (hybrid pathways $0 \rightarrow 1 \rightarrow 3$ and $0 \rightarrow 2 \rightarrow 3$) and n_{0123} (sequential pathway $0 \rightarrow 1 \rightarrow 2 \rightarrow 3$). Here, case (a) and case (b) results are different. See also Table 1. For case (b), the direct overtone pathway is found to be less important. Although the results obtained do not provide conclusive evidence of the importance of the direct-overtone pathway for the NO excitation from its ground state to $v = 3$ excited state, there is no question that the purely sequential mechanism is completely inadequate to explain that excitation.

We may also define a thermal limit of the sub-population analysis, which is shown in Fig. 1. Here we use the experimentally derived values of $\tau, \beta,$ and γ, and extrapolate to infinite interaction time. Again these results depend on the choice of case (a) or case (b) and they are shown in Table 1.

3.5 Comparison of IESH simulations to the kinetic model and experiment

The simulations with the IESH- based model were performed with the following incidence conditions: NO translational energy was 0.4 eV, NO rotational energy was 0.0 eV, NO vibrational energy was 0.12 eV (zero point energy). All trajectories were initiated with a random orientation of the NO molecule and with center-of-mass positions uniformly distributed in a slab of 1 Å thickness situated 10 Å above the surface. The initial linear momentum of NO was directed perpendicular to the surface. Several surface temperatures were chosen: 800K, 900K, 1000K and 1100K. $M_S = 80$ one-electronic surface states were populated with $N_e = 40$ electrons by means of sampling a Fermi-Dirac distribution. The phonons were allowed to reach equilibrium at the chosen value of T_S. Since the lowest measured excitation probability is on the order of 10^{-5}, we calculated one million trajectories for each value of T_S.

The results of the IESH calculations of absolute excitation probabilities are shown in Fig. 4 where they are compared to experimentally derived values. While the $0 \rightarrow 1$

excitation probabilities are reproduced by the IESH model quite well, some discrepancy appears for the $0 \rightarrow 2$ excitation probabilities, and it becomes even more pronounced for the $0 \rightarrow 3$ case. The deviation is particularly large at the highest values of T_S. This probably indicates that some aspects of the energy transfer mechanism are not reproduced well in the present implementation of the IESH simulation.

One possible problem could be related to the discretization of the electronic states of the metal, since the discretization may not be ideal over the wide energy range (0.7eV) necessary to describe $\Delta v = 1, 2$ and 3. We tested this hypothesis by carrying out a convergence study (with respect to M_S) of the excitation probabilities for production of $v = 1, 2$ and 3. See Fig. 6. Here, we show the results of IESH calculations carried out at $E_{\mathrm{i}} = 0.4$ eV and $T_S = 800$ K for M_s =10, 20, 40, 80 and 160. The experimental excitation probabilities are shown as horizontal dashed lines. For P_{01}, the results clearly converge by M_s=40. For P_{02} convergence is slower, being complete somewhere between M_s=80 and 160. For P_{03} the convergence is even slower and it is not entirely clear that it is even complete for M_s=160. Hence, we conclude that an improved discretization method is needed to obtain more accurate IESH results for multi-quantum vibrational energy transfer.

Beyond this rather banal problem, it may be that IESH does not capture the mechanism precisely. In other words, IESH may not lead to enough hybrid and direct overtone sub-population pathways. Put in another way, it may overestimate the importance of sequential pathways. To gain some insight into this, we have extracted information on population transfer pathways by analyzing individual trajectories producing v=3. We illustrate this in Fig.'s 7-9. Here, the time dependence of the energy deviation of the system's various degrees of freedom from their initial values is shown (upper panel). Example trajectories are shown of direct-overtone (Fig. 7), hybrid (Fig. 8) and sequential (Fig. 9) vibrational population transfer events. We also show the distances of the N and O atoms from the surface (lower panels) throughout the trajectories, which provide valuable information as to position and orientation of the NO molecule during a collision event. Here we analyze only three trajectories in detail. Systematic analysis of more trajectories will be presented in a future paper.

The trajectory shown in Fig. 7 shows a direct-overtone Δv=3 transition as described by the present implementation of IESH. Note that after approximately 1.25 ps, the

molecule has nearly enough kinetic energy (green line comes close to zero level) to leave the surface rotationally excited but vibrationally unexcited. However, the molecule fails to leave and re-collides with the surface. At $t = 2.08$ ps an electronic hop happens, which de-excites a hot EHP inducing a vibrational transition. This results in a vibrational excitation to NO of 0.7 eV (v=3). Note that there is also some loss of translational energy associated with the transition to v=3.

Fig. 8 shows a trajectory exhibiting hybrid behavior. Here, after 700 fs the NO molecule loses almost all of its incidence energy to the lattice. But during about 100 fs (between 1.1 and 1.2 ps on the plot) where the NO molecule was oriented approximately parallel to the surface, two hops occur de-exciting two hot EHPs of about 0.12 eV and 0.48 eV and pumping NO to v=3. In contrast to the previous case, the translational degrees of freedom of NO do not participate in the energy exchange and the molecule leaves the surface very slowly.

The sequential mechanism is illustrated by the trajectory shown in Fig. 9. Here, the collision event occurs in a similar way to the one shown in Fig. 8 with an important difference that now three successive hops can be observed.

We now make several qualitative comments about these three trajectories which are characteristic of the v=3 producing NO/Au collisions simulated by the present implementation of IESH. All of the v=3 producing trajectories exhibit strong energy oscillations between NO vibration (black lines in Fig. 7-9) and the lattice (gray lines). For example, this is clearly seen at 0.55±0.05 ps in Fig. 7. These oscillations are not due to vibrational coupling to EHPs. Rather they reflect formation of chemisorbed NO on Au, and this transient species' resulting redefined normal coordinates.

A dynamically important common feature of all trajectories producing v=3 is that at impact, a large amount of the incidence energy of translation is lost and transferred primarily to NO rotation and lattice degrees of freedom leading to secondary collisions of NO with the surface. The molecule typically spends more than half a picosecond at a distance of less than 1-2 Å from the surface with the N atom closer to the surface. As is clear from experimental angular distributions (Fig.1) there is no evidence for this sort of multi-bounce dynamic in any of the vibrationally inelastic NO/Au scattering. This clearly represents a shortcoming of the present implementation of the IESH model in describing $v = 0 \rightarrow 3$ scattering dynamics. Furthermore, this might explain why this model does not correctly describe the

incidence energy dependence of vibrational excitation for $v = 0 \rightarrow 1{,}2$ which were previously reported [6]. It, however, remains to a future work to see if our IESH simulations make similar multi-bounce errors for production of $v = 1$ and 2. At present, we have obtained angular distributions for all three vibrationally inelastic channels from IESH and these all appear broader than experiment, a result that is consistent with but must not necessarily be due to multi-bounce dynamics.

Another common feature of the trajectories that lead to $v = 3$ is that the excited vibrational state is always formed for molecules in the act of escaping the surface. One might describe this as an exit channel effect. The reasons for this are not fully clear; however, it does appear that in all seven of the IESH trajectories producing $v = 3$, only the last nonadiabatic event matters. In other words, vibrational excitations that occur in the entrance valley or in the strong coupling region close to the surface are quickly quenched. Whether this reflects the true dynamics of the system is doubtful. Indeed, it seems reasonable to assume that if the multi-bounce artifact in $v = 3$ production in IESH were removed, this behavior might also disappear.

Although we have not examined many trajectories in as full detail as just described, we have performed a mechanistic analysis for all of the trajectories leading to $v = 2$ and 3. By correlating the electronic de-excitation with the vibrational excitation for all trajectories producing NO $v = 2$ and $v = 3$, we could sort trajectories according to the various energy transfer pathways, i.e. sequential, hybrid and direct-overtone. See Table 1. The pathway contributions derived in this way disagree with those obtained from the kinetic model. For excitation to both $v = 2$ and $v = 3$, IESH predicts that sequential pathways dominate. We note in passing that this is remarkably close to the case (b) thermal limit expectation. Hence we conclude that (for whatever reasons that remain to be determined) the present implementation of IESH overestimates the importance of sequential excitation. Whether the tendency to overestimate sequential pathways is related to fundamental problems with the IESH approach or inadequacies in the PES and nonadiabatic couplings derived from DFT is not clear.

Regardless, this conclusion implies that if one were to compare IESH derived electronic energy distributions produced in vibrational relaxation to experiment, the IESH distribution would be less energetic. Indeed, if the reader will allow us to speculate, it is difficult to imagine how a theory that favors sequential pathways could ever explain vibrationally promoted election emission.

In summary, our comparison of the present implementation of IESH to the kinetic model, experiment as well as examination of individual trajectories leads us to several suggestions concerning potential improvements to the theory. First, for $v = 3$ production, unrealistic multiple bounce events seem to be required. This suggests that improvements to the PES are needed and that translation to phonon and rotational excitation may be too efficient in the model. How extensive this artifact of the model is in describing the higher probability events producing $v = 1$ and 2, remains to be examined. Second, IESH appears to unrealistically underestimate overtone and hybrid excitation pathways. This might be a result of the artifactual multi-bounce dynamics reported in this paper, again pointing to the need to improve the PES. Third, improvements in the treatment of the electronic continuum may be needed.

4. Conclusions

We measured the absolute probabilities for vibrational excitation of NO($v = 0 \rightarrow 1$, 2, and 3 in collisions with the (111) surface of a gold crystal at temperatures ranging from 300 to 1100 K. The probabilities exhibit an Arrhenius-type surface temperature dependence, indicating nonadiabatic coupling between NO vibration and thermally excited EHPs of the solid.

We extended a previously reported rate model to include four vibrational states and applied it to our data. Furthermore, the contributions of different pathways were calculated by means of a sub-population analysis. The measured $v = 2$ and $v = 3$ excitation probabilities do not agree with the assumption of a purely sequential excitation mechanism but rather indicate that direct first and hybrid transitions play an important role. Second overtone transitions cannot be ruled out.

A comparison of our results to first-principles IESH calculations showed that while the calculated values are quantitatively correct for $v = 1$ excitation, they under-predict $v = 2$ and especially $v = 3$ excitation for the higher surface temperatures, suggesting that the present implementation of an IESH-based simulation does not describe multi-quantum vibrational excitation correctly. There are also indications of mechanistic artifacts in the simulations, which favour multiple bounce dynamics for v=3 production in contrast to expectations from experimental angular distributions. Future work should investigate to what extent multiple bounce phenomena are important in the IESH-based model for $\Delta v = 1$ and 2. This might lead to a better

understanding of why the theory does not adequately capture the incidence energy dependence of vibrational excitation. Finally it appears that IESH converges more slowly with respect to the number of electronic states used in the discretization of the metal's continuum as Δv increases from +1 to +3. Improved treatments of the metals continuum might be helpful to improving IESH for future studies.

5. Acknowledgements

AMW, DJA and CB acknowledge support from the Alexander von Humboldt foundation. We would also like to thank Dr. Niel Shenvi and Prof. John Tully for helpful comments during this work and suggestions for improving this manuscript.

6. References

1. (a) Wodtke, A. M.; Tully, J. C.; Auerbach, D. J., Electronically Non-Adiabatic Interactions of Molecules at Metal Surfaces: Can We Trust the Born-Oppenheimer Approximation for Surface Chemistry? *Int. Rev. Phys. Chem.* **2004,** *23* (4), 513-539; (b) Hasselbrink, E., How Non-Adiabatic Are Surface Dynamical Processes? *Current Opinion in Solid State & Materials Science* **2006,** *10* (3-4), 192-204; (c) Wodtke, A. M.; Matsiev, D.; Auerbach, D. J., Energy Transfer and Chemical Dynamics at Solid Surfaces: The Special Role of Charge Transfer. *Prog. Surf. Sci.* **2008,** *83* (3), 167-214; (d) Rahinov, I.; Cooper, R.; Matsiev, D.; Bartels, C.; Auerbach, D. J.; Wodtke, A. M., Quantifying the Breakdown of the Born-Oppenheimer Approximation in Surface Chemistry. *PCCP* **2011,** *13* (28), 12680-12692; (e) Bartels, C.; Cooper, R.; Auerbach, D. J.; Wodtke, A. M., Energy Transfer at Metal Surfaces: The Need to Go Beyond the Electronic Friction Picture. *Chemical Science* **2011,** *2* (9), 1647-1655.

2. (a) Huang, Y. H.; Rettner, C. T.; Auerbach, D. J.; Wodtke, A. M., Vibrational Promotion of Electron Transfer. *Science* **2000,** *290* (5489), 111-114; (b) White, J. D.; Chen, J.; Matsiev, D.; Auerbach, D. J.; Wodtke, A. M., Conversion of Large-Amplitude Vibration to Electron Excitation at a Metal Surface. *Nature* **2005,** *433* (7025), 503-505; (c) Nahler, N. H.; White, J. D.; LaRue, J.; Auerbach, D. J.; Wodtke, A. M., Inverse Velocity Dependence of Vibrationally Promoted Electron Emission from a Metal Surface. *Science* **2008,** *321* (5893), 1191-1194.

3. (a) Rettner, C. T.; Fabre, F.; Kimman, J.; Auerbach, D. J., Observation of Direct Vibrational-Excitation in Gas-Surface Collisions - No on Ag(111). *Physical Review Letters* **1985,** *55* (18), 1904-1907; (b) Watts, E. K.; Siders, J. L. W.; Sitz, G. O., Vibrational Excitation of No Scattered from Cu(110). *Surf. Sci.* **1997,** *374* (1-3), 191-196; (c) Cooper, R.; Rahinov, I.; Li, Z. S.; Matsiev, D.; Auerbach, D. J.; Wodtke, A. M., Vibrational Overtone Excitation in Electron Mediated Energy Transfer at Metal Surfaces. *Chemical Science* **2010,** *1* (1), 55-61.

4. (a) Shenvi, N.; Roy, S.; Parandekar, P.; Tully, J., Vibrational Relaxation of No on Au(111) Via Electron-Hole Pair Generation. *J. Chem. Phys.* **2006,** *125* (15), 154703; (b) Monturet, S.; Saalfrank, P., Role of Electronic Friction During the Scattering of Vibrationally Excited Nitric Oxide Molecules from Au(111). *Physical Review B* **2010,** *82* (7), 075404; (c) Kasai, H.; Okiji, A., Electron-Hole Pair Mechanism for Excitation of Intramolecular Vibrations in Molecule Surface Scattering. *Surf. Sci.* **1990,** *225* (1-2), L33-L38.

5. (a) Newns, D. M., Electron-Hole Pair Mechanism for Excitation of Intramolecular Vibrations in Molecule Surface Scattering. *Surf. Sci.* **1986,** *171* (3), 600-614; (b) Gadzuk, J. W.; Holloway, S., Vibrational Excitation in Gas-Surface Collisions. *Physical Review B* **1986,** *33* (6), 4298-4300.

6. Cooper, R.; Bartels, C.; Kandratsenka, A.; Rahinov, I.; Shenvi, N.; Golibrzuch, K.; Li, Z.; Auerbach, D. J.; Tully, J. C.; Wodtke, A. M., Multiquantum Vibrational Excitation of No Scattered from Au(111): Quantitative Comparison of Benchmark Data to Ab Initio Theories of Nonadiabatic Molecule–Surface Interactions. *Angew. Chem. Int. Ed.* **2012,** *124* (20), 5038–5042.

7. Matsiev, D.; Li, Z.; Cooper, R.; Rahinov, I.; Bartels, C.; Auerbach, D. J.; Wodtke, A. M., On the Temperature Dependence of Electronically Non-Adiabatic Vibrational Energy Transfer in Molecule-Surface Collisions. *PCCP* **2011,** *13*, 8153-8162.

8. Ran, Q.; Matsiev, D.; Wodtke, A. M.; Auerbach, D. J., An Advanced Molecule-Surface Scattering Instrument for Study of Vibrational Energy Transfer in Gas-Solid Collisions. *Rev Sci Instrum* **2007,** *78* (10).

9. Rahinov, I.; Cooper, R.; Yuan, C.; Yang, X.; Auerbach, D. J.; Wodtke, A. M., Efficient

Vibrational and Translational Excitations of a Solid Metal Surface: State-to-State Time-of-Flight Measurements of Hcl(V = 2,J = 1) Scattering from Au(111). *J. Chem. Phys.* **2008,** *129* (21), 214708.

10. Cooper, R.; Li, Z. S.; Golibrzuch, K.; Bartels, C.; Rahinov, I.; Auerbach, D. J.; Wodtke, A. M., On the Determination of Absolute Vibrational Excitation Probabilities in Molecule-Surface Scattering: Case Study of No on Au(111). *Journal of Chemical Physics* **2012,** *137* (6), 064705-12.

11. Hippler, M.; Pfab, J., Detection and Probing of Nitric Oxide (No) by Two-Colour Laser Photoionisation (Rempi) Spectroscopy on the a←X Transition. *Chem. Phys. Lett.* **1995,** *243* (5-6), 500-505.

12. (a) Shenvi, N.; Roy, S.; Tully, J. C., Nonadiabatic Dynamics at Metal Surfaces: Independent-Electron Surface Hopping. *J. Chem. Phys.* **2009,** *130* (17), 174107; (b) Roy, S.; Shenvi, N. A.; Tully, J. C., Model Hamiltonian for the Interaction of No with the Au(111) Surface. *J. Chem. Phys.* **2009,** *130* (17), 174716.

13. Tully, J. C., Molecular Dynamics with Electronic Transitions. *J. Chem. Phys.* **1990,** *93* (2), 1061-1071.

14. (a) Burkey, R. S.; Cantrell, C. D., Discretization in the Quasi-Continuum. *Journal of the Optical Society of America B-Optical Physics* **1984,** *1* (2), 169-175; (b) Kazansky, A. K., Precise Analysis of Resonance Decay Law in Atomic Physics. *Journal of Physics B: Atomic, Molecular and Optical Physics* **1997,** *30* (6), 1401-1410; (c) Shenvi, N.; Schmidt, J. R.; Edwards, S. T.; Tully, J. C., Efficient Discretization of the Continuum through Complex Contour Deformation. *Physical Review A* **2008,** *78* (2).

15. Billing, G. D., *Dynamics of Molecule Surface Interactions*. John Wiley & Sons: 2000.

16. Gorbachev, Y. E.; Gordillo-Vázquez, F. J.; Kunc, J. A., Diameters of Rotationally and Vibrationally Excited Diatomic Molecules. *Physica A* **1997,** *247* (1-4), 108-120.

17. Cooper, R.; Li, Z.; Golibrzuch, K.; Bartels, C.; Rahinov, I.; Auerbach, D. J.; Wodtke, A. M., On the Determination of Absolute Vibrational Excitation Probabilities in Molecule-Surface Scattering: Case Study of No on Au(111). *J. Chem. Phys.*, accepted for publication.

18. Zacharias, H.; Rougemont, F. d.; Heinz, T. F.; Loy, M. M. T., Ionization Probabilities of a [Sup 2] Sigma [Sup +](V[Prime]=0,1,2) and B [Sup 2] Pi(V[Prime]=0,2) States of No. *The Journal of Chemical Physics* **1996,** *105* (1), 111-117.

19. Saakyan, A. S.; Butayev, B. S.; Spiridonov, V. P., A Simple Analytical Approximation for the Vibrational Partition Function of Diatomic Systems. *Chem Phys Lett* **1986,** *123* (3), 222-225.

7. Tables

Channel	Kinetic model[i]		Thermal limit[iii]		IESH[iv]
	(a)[ii]	(b)[ii]	(a)[ii]	(b)[ii]	
	$v = 0 \rightarrow 2$				
Sequential	28	49	63	79	81
Direct-overtone	71	49	37	21	19
	$v = 0 \rightarrow 3$				
Sequential	6±1	23±1	34	53	62±14
Hybrid	41±1	71±2	49	37	31±10
Direct-overtone	53±2	5±3	17	10	7±5

Table 1: Contributions of different pathways to the excitation of $\boldsymbol{v = 2,3}$ at $\boldsymbol{T_S =}$ **800**K. *The contributions are given in percent. The estimated uncertainties for the kinetic model results are calculated from the uncertainties in fit parameters (eq. (13)) and shown when they are larger than 0.5%.*

[i] results of sub-population analysis. See. Sections 2.2 and 2.3.

[ii] indicates the assumption-case concerning $v -$ scaling of the nonadiabatic coupling.

[iii] The results of the sub-population analysis in the limit $t_{int} \rightarrow \infty$.

[iv] The present implementation of IESH follows Ref. 6 and 12.

8. Figures

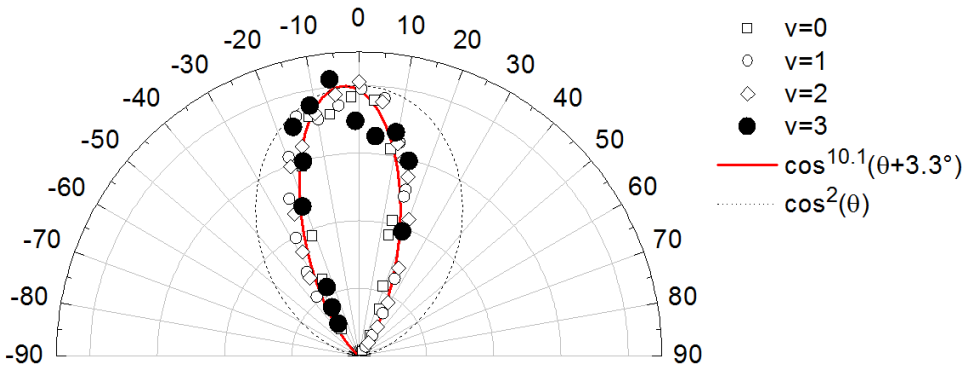

Figure 1: Angular distributions of scattered NO(v) molecules. Open symbols: v=0, 1, 2 experimental data; solid symbols: $v = 3$ experimental data; dotted line: $cos^2\theta$ distribution expected for trapping-desorption under our conditions; solid line: $cos^{10.1}(\theta + 3.3°)$ fit function. The absolute intensities were normalized to one another to emphasize the shape of the angular distribution. T_S = 1073 K for v =1, 2, 3 and 315 K for $v = 0$.

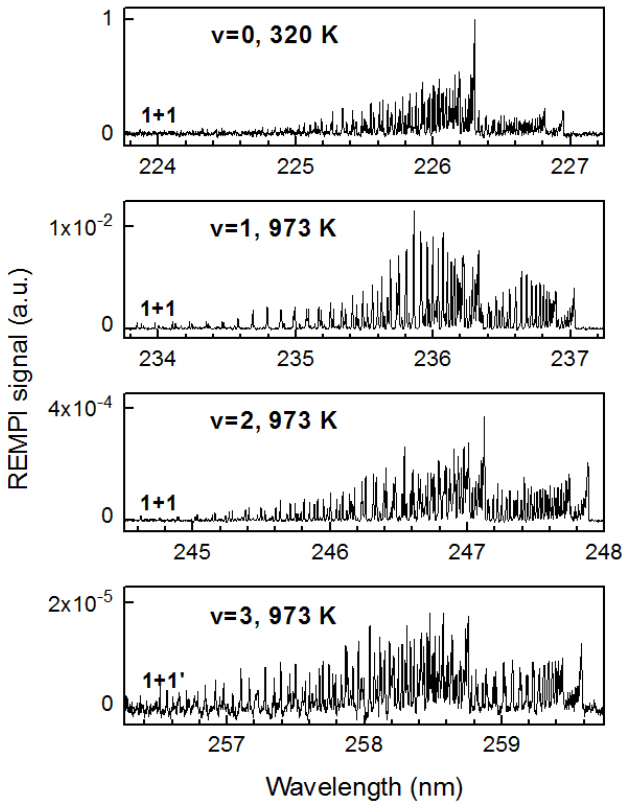

Figure 2: Typical REMPI spectra of scattered NO($v = 0 \rightarrow v' = 1, 2, 3$). The A-X(0-0, 0-1 and 0-2) bands were employed using one-color (1+1) REMPI while the A-X(0-3) band was utilized using two-color (1+1') REMPI. The recorded spectra were corrected for differences in MCP gain, laser power, and for the two-color REMPI enhancement factor for the A-X(0-3) band. Note that the dynamic range of the measurement attainable using both REMPI schemes spans over ~5 orders of magnitude.

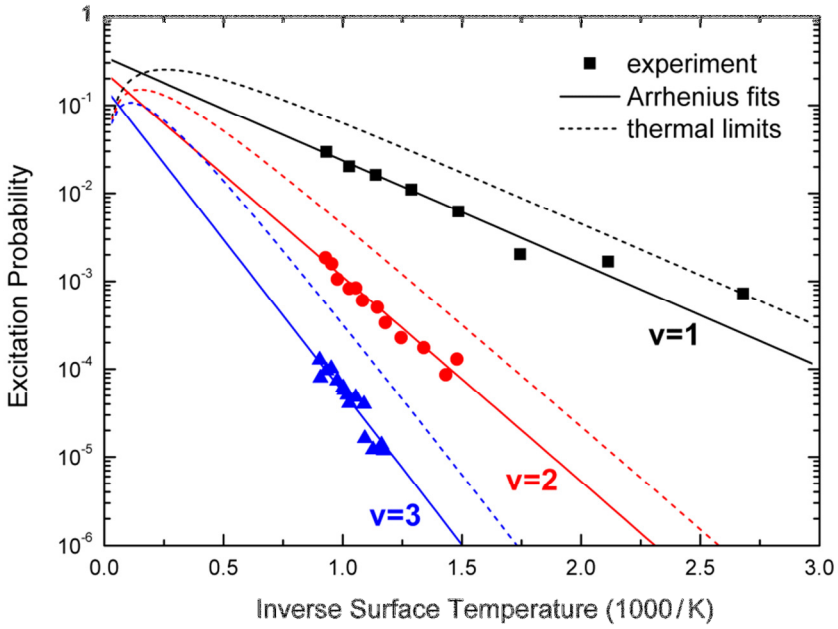

Figure 3: Arrhenius plots of absolute excitation probabilities for $v = 1$, 2, and 3. Experimental results: black are $v = 1$, red are $v = 2$, blue are $v = 3$). Solid lines: fits to Arrhenius expression (Eq. 11) with activation energy fixed to vibrational excitation energy. Dashed lines: thermal limit (Eq. 12).

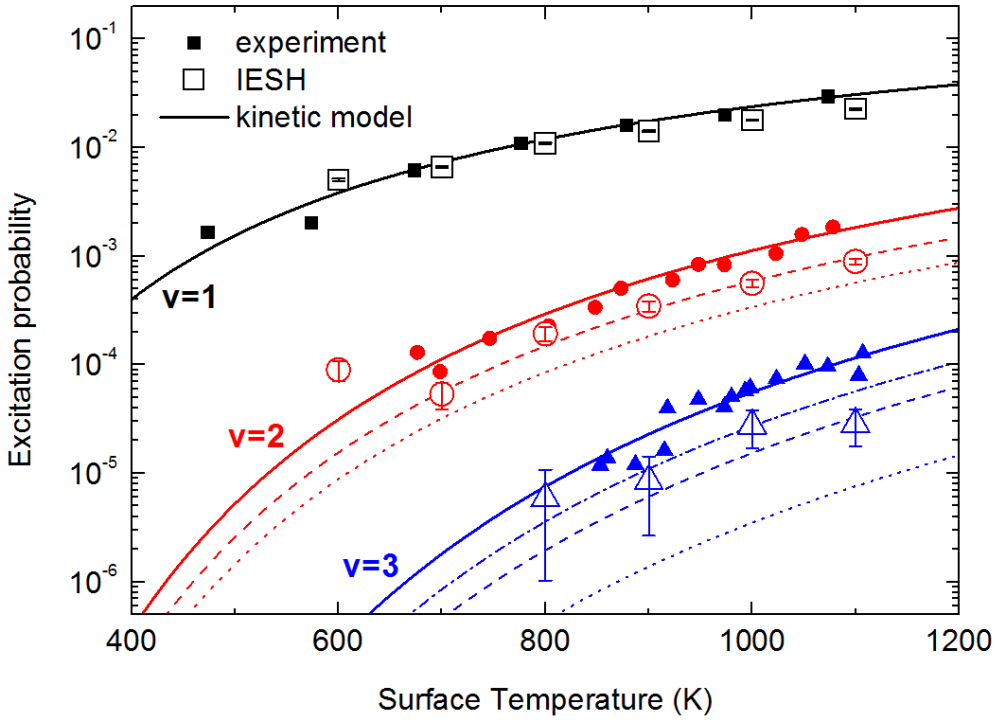

Figure 4: Comparison of the IESH theory to the measured absolute vibrational excitation probabilities fitted with the kinetic state-to-state model. Closed symbols are experimentally obtained absolute excitation probabilities. P_{01}, P_{02} *and* P_{03} *(black squares:* $v = 1$, *red circles:* $v = 2$, *blue triangles:* $v = 3$*). Case (a) and case (b) results are identical. See text. The kinetic model fit allowing for only sequential pathways of vibrational excitation, i.e. with* $\beta = \gamma = 0$ *is shown by dotted – case (a) – and dashed – case (b) – curves. The dot-dashed line results from a fit with the second overtone switched off, i.e. with* $\gamma = 0$*, case (a). Open symbols are predictions of presently implemented IESH-based model (black squares:* $v = 1$, *red circles* $v = 2$, *blue triangles* $v = 3$*). The error bars on the IESH data represent a 95% confidence interval.*

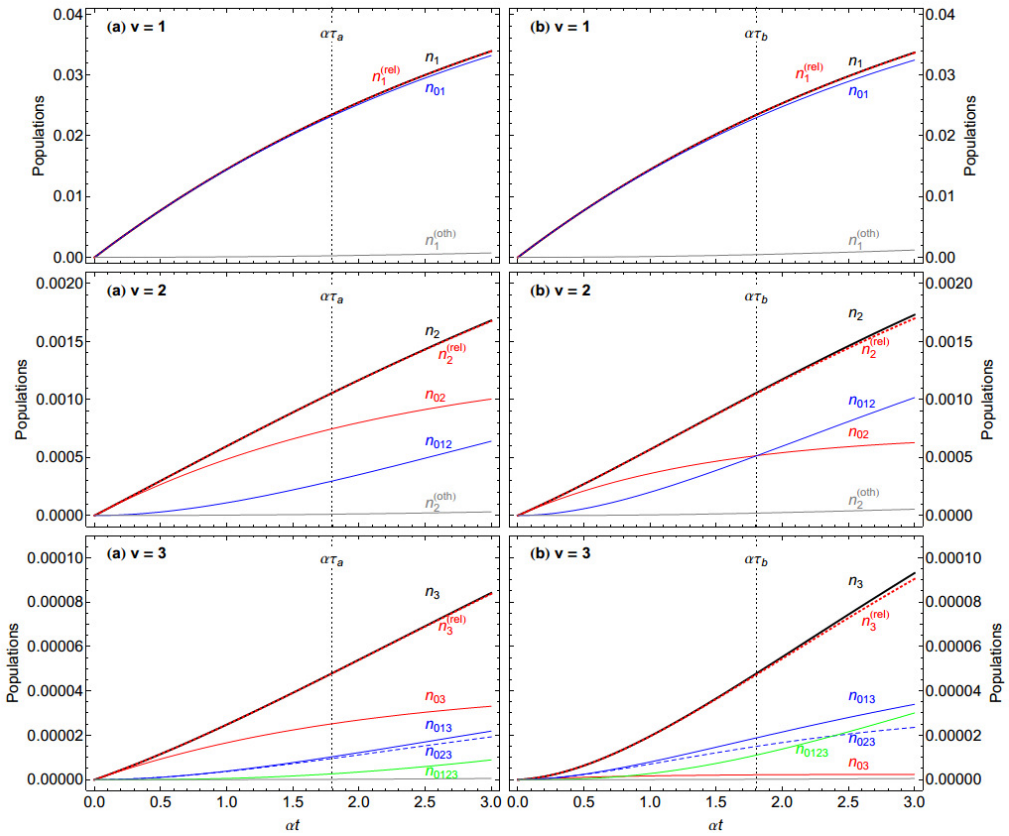

Figure 5: Sub-populations as functions of dimensionless time, $\boldsymbol{\alpha t}$, for $\boldsymbol{T_S = 800}$K. *The kinetic model was employed to fit absolute excitation probabilities derived from experiment. The sub-population analysis was performed as described in section 2.3. Two assumptions about the vibrational quantum number,* $\boldsymbol{v}$, *dependent scaling of the state-to-state coupling are employed. Case (a) assumes* $\boldsymbol{v}$ *independent scaling – left column. Case (b) assumes scaling linearly proportional to* $\boldsymbol{v}$, *right column. See text. The value of* $\boldsymbol{\alpha t}$*=1.8 is marked to indicate the effective collision time derived from these experiments.*

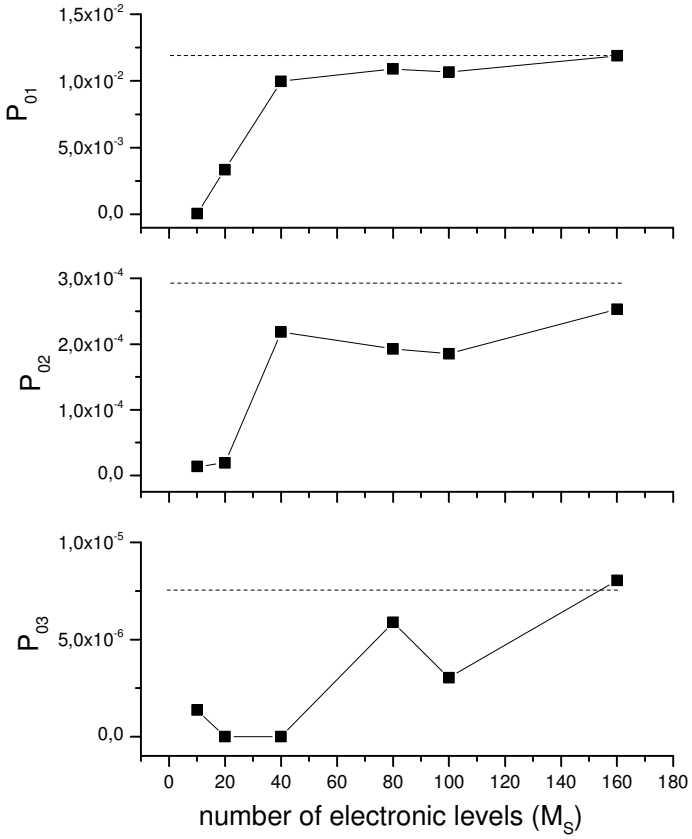

Figure 6: The effect of the number of electronic levels, $\boldsymbol{M_S}$, used in IESH simulations on the calculated vibrational excitation probabilities. Solid symbols: probabilities calculated from IESH at $\boldsymbol{E_i = 0.4}$ eV and $\boldsymbol{T_S = 800}$ K; dashed lines show the corresponding experimentally derived values. Increasing the number of levels leads to higher excitation probabilities and thus to a better agreement with experiment. Convergence is slower for higher values of $\boldsymbol{v}$.

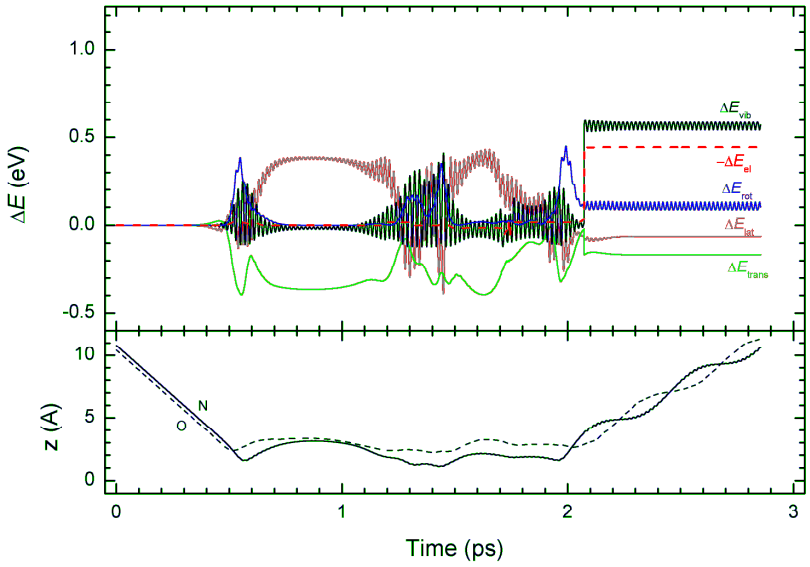

Figure 7: An IESH trajectory for NO ($\boldsymbol{v} = \mathbf{0}$) scattering from Au(111) demonstrating the direct-overtone vibrational excitation channel. NO incidence energy is 0.4 eV and $\boldsymbol{T_S}$ =800 K. Final NO vibrational energy value corresponds to $\boldsymbol{v}$ =3 excitation. Upper panel shows the NO translational energy, $\boldsymbol{\Delta E_{tr}}$ (green), NO rotational energy, $\boldsymbol{\Delta E_{rot}}$ (blue), NO vibrational energy, $\boldsymbol{\Delta E_{vib}}$ (black), lattice phonon energy, $\boldsymbol{\Delta E_{lat}}$ (grey) and electronic energy, $\boldsymbol{\Delta E_{el}}$ (red, dashed) referenced to their initial values. The change in the electronic energy is taken with the negative sign in order to more easily compare the electronic-vibrational energy resonant transfer. The lower panel shows the distance of N atom (solid line) and O atom (dashed line) from the surface as a function of time.

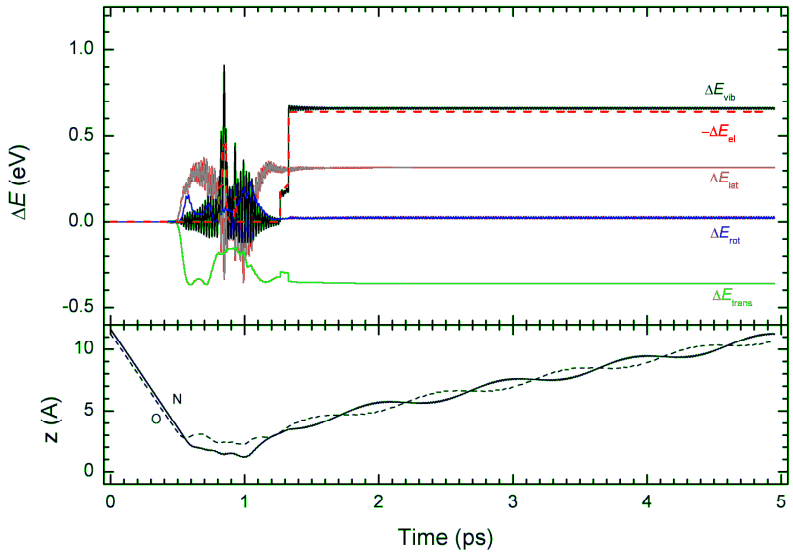

Figure 8: An IESH trajectory for NO ($\boldsymbol{v} = \mathbf{0}$) scattering from Au(111) demonstrating the hybrid vibrational excitation channel. Notations are the same as in Fig. 7.

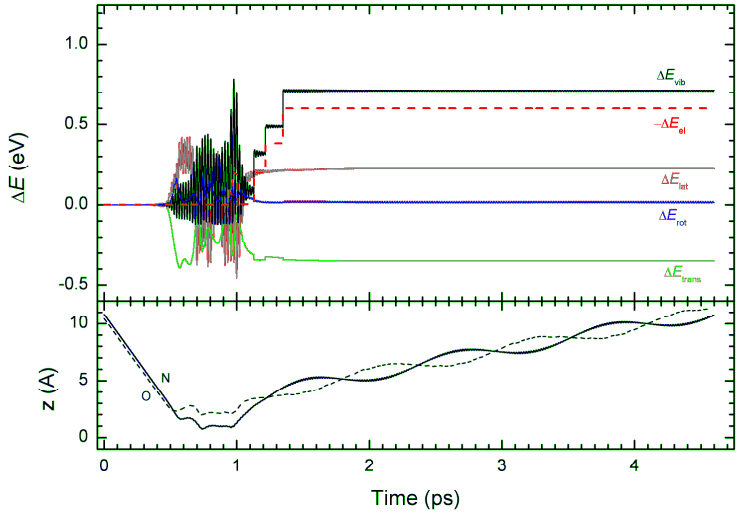

Figure 9: An IESH trajectory for NO ($\boldsymbol{v} = \mathbf{0}$) scattering from Au(111) demonstrating the sequential vibrational excitation channel. Notations are the same as in Fig. 7.

9. Appendix:

Validity of Equation (12) (thermal limits) for anharmonic oscillator

In a thermal equilibrium with a bath at the temperature T the probability to find a system in the state n with energy E_n is proportional to the Boltzmann factor:

$$P_n = Q^{-1} e^{-\beta E_n} \tag{A1}$$

where $\beta = (k_B T)^{-1}$ and the normalization factor is a partition function

$$Q = \sum_n e^{-\beta E_n}$$

In case of a harmonic oscillator with energy levels

$$\frac{E_n}{hc} = \omega_e \left(n + \frac{1}{2}\right) \tag{A2}$$

the sum defining the partition function can be calculated exactly yielding

$$Q_h = \frac{e^{-\frac{1}{2}\beta hc\omega_e}}{1 - e^{-\beta hc\omega_e}} \tag{A3}$$

For an anharmonic oscillator with the anharmonicity described by the spectroscopic energy formula

$$\frac{E_n}{hc} = \omega_e \left(n + \frac{1}{2}\right) - \omega_e x_e \left(n + \frac{1}{2}\right)^2 \tag{A4}$$

the corresponding partition function can also be represented analytically by a rather simple expression[19]

$$Q = Q_h e^{\frac{1}{4}\beta hc\omega_e x_e} \left[1 + \gamma(\beta) e^{-\beta hc\omega_e}\right]$$

where

$$\gamma(\beta) = \sum_{k=1}^{\infty} \frac{b_k}{k!} \left[\frac{2\beta hc\omega_e x_e}{(1 - e^{-\beta hc\omega_e})^2}\right]^k$$

is the convergent infinite series with

$$b_1 = 1, \qquad b_2 = 1 + 4e^{-\beta hc\omega_e} + e^{-2\beta hc\omega_e}, \ldots$$

This series converges very rapidly and even in 0^{th} order, when $\gamma(\beta) = 0$ and the partition function

$$Q_0 = Q_h e^{\frac{1}{4}\beta hc\omega_e x_e} = \frac{e^{-\beta hc\left(\frac{\omega_e}{2} - \frac{\omega_e x_e}{4}\right)}}{1 - e^{-\beta hc\omega_e}} \tag{A5}$$

the approximation works quite well.

Now, going back to the probability definition (A1) it is easy to observe that rescaling the Boltzmann factor by some (in general, temperature-dependent) scaling factor, $f(\beta)$, does not change that probability:

$$P_n' = \frac{f(\beta)e^{-\beta E_n}}{\sum_n f(\beta)e^{-\beta E_n}} = \frac{f(\beta)e^{-\beta E_n}}{f(\beta)\sum_n e^{-\beta E_n}} = \frac{e^{-\beta E_n}}{\sum_n e^{-\beta E_n}} = P_n$$

An interesting special form of the scaling factor $f(\beta) = e^{-a\beta}$ corresponds to shifting the energy values by a constant a which does not influence the observables.

Observing that the denominators of partition functions (A3) and (A5) are equal, we define a scaling factor in case of harmonic and anharmonic oscillator to be

$$f_h(\beta) = \exp\left(-\frac{1}{2}\beta hc\omega_e\right), \text{and } f_0(\beta) = \exp\left(-\beta hc\left(\frac{\omega_e}{2} - \frac{\omega_e x_e}{4}\right)\right),$$

respectively, thus, shifting a zero of energy to the value of zero-point energy (which can be found from corresponding formulae for energy levels of harmonic (A2) and anharmonic (A4) oscillators).

Taking these shifts into account, we can rewrite Eq. (A1) defining the excitation probability in the form ($E_{0n} = E_n - E_0$)

$$P_n = e^{-\beta E_{0n}}(1 - e^{-\beta hc\omega_e})$$

which is the same for harmonic and anharmonic oscillators differing in the starting point of energy only.

So, the formula for the thermal limit of excitation probability (12) is valid not only for the harmonic oscillator, but for the anharmonic one, too.

Graphic for the Table of Contents: